



Article

Nanotoxicity of 2D Molybdenum Disulfide, MoS₂, Nanosheets on Beneficial Soil Bacteria, *Bacillus cereus* and *Pseudomonas aeruginosa*

Michael Bae ^{1,†}, Jun Kyun Oh ^{2,†}, Shuhao Liu ¹, Nirup Nagabandi ¹, Yagmur Yegin ¹, William DeFlorio ¹, Luis Cisneros-Zevallos ^{3,4} and Ethan M. A. Scholar ^{1,5,*}

¹ Artie McFerrin Department of Chemical Engineering, Texas A&M University, College Station, TX 77843, USA; bsy7790@tamu.edu (M.B.); liushuhao1993@tamu.edu (S.L.); nirup.nagabandi@essentium.com (N.N.); yagmur-ravli@tamu.edu (Y.Y.); wdeflorio@tamu.edu (W.D.)

² Department of Polymer Science and Engineering, Dankook University, 152 Jukjeon-ro, Suji-gu, Yongin-si 16890, Gyeonggi-do, Korea; junkyunoh@dankook.ac.kr

³ Department of Nutrition and Food Science, Texas A&M University, College Station, TX 77843, USA; lcisnero@tamu.edu

⁴ Department of Horticultural Science, Texas A&M University, College Station, TX 77843, USA

⁵ Department of Materials Science and Engineering, Texas A&M University, College Station, TX 77843, USA

* Correspondence: ethanscholar@tamu.edu

† Both authors contributed equally to this work.



Citation: Bae, M.; Oh, J.K.; Liu, S.; Nagabandi, N.; Yegin, Y.; DeFlorio, W.; Cisneros-Zevallos, L.; Scholar, E.M.A. Nanotoxicity of 2D Molybdenum Disulfide, MoS₂, Nanosheets on Beneficial Soil Bacteria, *Bacillus cereus* and *Pseudomonas aeruginosa*. *Nanomaterials* **2021**, *11*, 1453. <https://doi.org/10.3390/nano11061453>

Academic Editor: Emmanuel Flahaut

Received: 30 March 2021

Accepted: 26 May 2021

Published: 31 May 2021

Publisher's Note: MDPI stays neutral with regard to jurisdictional claims in published maps and institutional affiliations.



Copyright: © 2021 by the authors. Licensee MDPI, Basel, Switzerland. This article is an open access article distributed under the terms and conditions of the Creative Commons Attribution (CC BY) license (<https://creativecommons.org/licenses/by/4.0/>).

Abstract: Concerns arising from accidental and occasional releases of novel industrial nanomaterials to the environment and waterbodies are rapidly increasing as the production and utilization levels of nanomaterials increase every day. In particular, two-dimensional nanosheets are one of the most significant emerging classes of nanomaterials used or considered for use in numerous applications and devices. This study deals with the interactions between 2D molybdenum disulfide (MoS₂) nanosheets and beneficial soil bacteria. It was found that the log-reduction in the survival of Gram-positive *Bacillus cereus* was 2.8 (99.83%) and 4.9 (99.9988%) upon exposure to 16.0 mg/mL bulk MoS₂ (macroscale) and 2D MoS₂ nanosheets (nanoscale), respectively. For the case of Gram-negative *Pseudomonas aeruginosa*, the log-reduction values in bacterial survival were 1.9 (98.60%) and 5.4 (99.9996%) for the same concentration of bulk MoS₂ and MoS₂ nanosheets, respectively. Based on these findings, it is important to consider the potential toxicity of MoS₂ nanosheets on beneficial soil bacteria responsible for nitrate reduction and nitrogen fixation, soil formation, decomposition of dead and decayed natural materials, and transformation of toxic compounds into nontoxic compounds to adequately assess the environmental impact of 2D nanosheets and nanomaterials.

Keywords: MoS₂ nanomaterials; 2D nanosheets; nanotoxicity; soil bacteria

1. Introduction

Prior research has indicated that engineered nanomaterials, such as quantum dots, nanoparticles, nanowires, nanorods, and nanosheets, can be released to the environment contingently during their life cycles (product use, disposal, and weathering) [1]. The increasing use of engineered nanomaterials has led to an increasing concern on their possible build-up in the environment, and sequentially in the food supply [2,3]. Although various unique properties of nanomaterials have made them attractive in numerous applications, some of these properties, such as enhanced transport, increased bioavailability, enlarged surface area, and greater surface reactivity, can adversely impact living organisms and microorganisms [4]. For example, Dimkpa et al. [5] investigated the effect of CuO (<50 nm) and ZnO (<100 nm) NPs on wheat (*Triticum aestivum*) grown in a solid matrix (sand). They reported oxidative stress in NP-treated plants, which was proven by increased lipid peroxidation and oxidized glutathione in roots and decreased chlorophyll content in shoots,

and higher peroxidase and catalase activities in roots. Xin et al. [6] reported that silver nanoparticles can modify the expression profiles of neural development-related genes (*gfap*, *huC* and *ngn1*), metal-sensitive metallothioneins, and ABCC genes in exposed zebrafish embryos. However, the majority of previous efforts with environmental implications of nanomaterials on living organisms have primarily focused on metal and metal oxide nanomaterials, as well as carbon-based nanomaterials such as fullerenes, graphene, and carbon nanotubes (CNTs) [7–11].

Recently, among various types of nanomaterials, 2D nanosheets such as graphene, hexagonal BN, MoS₂, WS₂, MgO₂, MXenes, owing to their ultrahigh aspect ratio and unusual optical, electronic, thermal, and mechanical properties, have gained particular attention from scientists and engineers [12–16]. Rapidly emerging applications relying on 2D nanosheets include electrodes for energy storage devices [17], lubricants and friction reducers [18], thermal management materials, [15], sensors [19], membranes for gas separation [20], water purification systems [21], composite structural materials [22], and oil cleanup systems [23]. With an increasing number of applications and utilization, it is essential to study and understand the interactions of 2D nanosheets with living organisms and environmental surfaces in order to assess the impact of such nanomaterials on the environment. Accordingly, many studies have recently investigated the interactions of 2D nanosheets (primarily graphene) and living organisms such as plants, animals, algae, and bacteria [24–26].

Molybdenum disulfide (MoS₂) nanosheets, which are relatively new types of 2D nanomaterials, have received increased attention after the peak graphene and hexagonal boron nitride (h-BN) era. The bulk form of MoS₂ exhibits randomly stratified poly-structures because of its hexagonal monolayers bound to each other via Van der Waals forces [12]. The hexagonal monolayer of MoS₂ has a transition metal in the middle, sandwiched by two layers of chalcogenide atoms with a stable covalent bonding [27]. The bulk MoS₂ has a stacked multilayer form in nature, which can readily be exfoliated into fewer layers with the exertion of mechanical force or agitation [28,29]. MoS₂ nanosheets have the ability to act as a catalyst for generating hydrogen [30,31], which can be applied to hydro-desulfurization processes in industry [32]. The enhanced bandgap of MoS₂ nanosheets (1.8 eV) has been associated in photoelectric reactions [33,34]. The capability of disinfecting water by harvesting the whole spectrum of visible light from the sun has also been noted as one of the applications with MoS₂ nanosheets [35]. The ability to prevent bacterial biofilms with MoS₂ particles (90 nm and 2–6 μm) and surfaces has recently been reported [36].

Soil bacteria are a fundamental and integral part of soil ecological systems. They control carbon dynamics, nutrient cycles, nitrification and denitrification, the early stages of decomposition of organic materials, and plant productivity [37,38]. In addition, they take up and transform toxic compounds into nontoxic compounds via immobilization [39,40]. Therefore, plausibly, recent studies have focused on the impact of engineered nanomaterials on soil bacteria. Disruption of cell walls, hydrophobic interactions with cell membranes, and the dissolution/release of metals have been proposed as mechanisms for the nanotoxicity of engineered nanomaterials such as CuO, ZnO, MgO, CeO₂ nanoparticles (NPs) on soil bacteria [41–43]. Whiteside et al. [44] and Moll et al. [45] found that CdSe/ZnO quantum dots and CeO₂, TiO₂ NPs had no effect on nitrogen-fixing bacteria nodulation, while Sillen et al. [43] found significant differences in bacterial community carbon use and lowered enzymatic activity upon exposure to ZnO, CeO₂ NPs. However, studies focusing on how MoS₂ nanosheets interact with soil bacteria and what their potential toxic effects are on soil bacteria have not been reported, to the best of our knowledge.

In this work, we investigated the growth dynamics of Gram-positive *Bacillus cereus* and Gram-negative *Pseudomonas aeruginosa* under the influence of bulk MoS₂ and 2D MoS₂ nanosheets as a function of concentration and exposure time. *B. cereus* was chosen as the model soil bacteria because they are involved in nitrification processes, phosphate transport, protection of the rhizosphere from fungal diseases, and heavy metal remediation [46–48]. *P. aeruginosa* was selected as another model soil bacteria in this study because

they play a central role in nitrate reduction and the decomposition of toxic compounds in soil [49,50]. Bacterial growth behavior in the presence and absence of bulk MoS₂ and 2D MoS₂ nanosheets were investigated using the agar plating assay. Then, by analyzing concentration-dependent bacterial survival data, the median effective concentration (EC₅₀), corresponding to the concentration of bulk and nanoexfoliated MoS₂ which induces a response halfway between the baseline and maximum after 8 h of exposure time, was calculated for each microorganism from the dose–response curve. Scanning electron microscopy was used to obtain complementary information on how bulk and nanoexfoliated MoS₂ influences bacterial morphology. Zeta potential measurements were conducted to gain insights into the nature of intermolecular interactions between MoS₂ and soil bacteria.

2. Materials and Methods

2.1. Preparation of MoS₂ Nanosheets

Molybdenum (IV) disulfide, 99% (metal basis) powder was purchased from Alfa Aesar (CAS No. 41827, Haverhill, MA, USA) (Table S1). After MoS₂ was added to deionized water (DI) water at a concentration of 16 mg/mL, high-intensity ultrasonication was utilized to exfoliate bulk materials into nanosheets via a probe sonicator (SJIA-2000W, Ningbo Haishu Sklon Electronics Instruments Co., Zhejiang, China). The exfoliation was achieved at a sonication power of 2000 W and frequency of 19.5–20.5 Hz with one hour of ultrasonication (3 s on and 1 s off cycles). All of these processes were carried out in an ice bath to eliminate the possibility of temperature-induced oxidation of MoS₂ (The exfoliated MoS₂ in water information is uploaded in Figures S1 and S2). On the other hand, to prepare the bulk controls, the bulk suspension was centrifuged at 4000 rpm for 15 min (AccuSpin 400, Thermo Fisher Scientific, Waltham, MA, USA) to separate nanoscale materials from the supernatant layer, and the same volume of water was compensated.

2.2. Bacterial Cultures and Plate Counting

Two soil bacteria, Gram-positive *Bacillus cereus* (ATCC 14579) and Gram-negative *Pseudomonas aeruginosa* (ATCC 9027), were used in this study. Experimental cultures of these were transferred by using the tip of an inoculating loop (CAS No. 12000-812, VWR, 10 µL, sterile), from tryptic soy agar (TSA; Becton, Dickinson and Co., Franklin Lakes, NJ, USA) slant with grown colonies to the culturing centrifuge tube which contained 9 mL of tryptic soy broth (TSB; Becton, Dickinson and Co., Franklin Lakes, NJ, USA). The tubes of these bacteria were incubated aerobically at 37 °C for 24 h without shaking. Next, an inoculating loop transferred 10 µL from the 9 mL of tryptic soy broth with bacteria to a fresh 9 mL of tryptic soy broth medium. This process repeated up to three times. Second and third transfers of the culture were cleaned with sterilized DI water for twice after performing centrifugation for 15 min each with 4000 rpm to remove the supernatant part of tryptic soy broth and replacing it with sterilized DI water twice, then refilling it with 1 g/L peptone (Becton, Dickinson and Co., Franklin Lakes, NJ, USA) water in the end. The final growth in the culture media after plate counting was $6.48 \pm 0.15 \log_{10}$ CFU/mL for *B. cereus* and $8.49 \pm 0.08 \log_{10}$ CFU/mL for *P. aeruginosa* by stirring them with a magnetic bar for 24 h at room temperature, transferring 1 mL to a Petri dish, mixing them with TSA, and incubating them again for 24 h at 37 °C and counting the number of the colonies on the agar (Figure S3).

2.3. Characterization of Soil Bacteria

For characterization, (100) silicon wafers were cut into 10 mm × 10 mm pieces and then polished by piranha solution with a 3:1 mixture of sulfuric acid and 30% hydrogen peroxide for 1 h, washed with ultrapurified water, and left to dry at 23 °C. The cultured bacteria that were diluted in sterilized DI water at a volumetric ratio of 1000:1 were drop-cast with 1–3 drops using a micropipette (100 µL) to cover the silicon wafer surface, exposed to a trace amount of acrolein, dried for one day inside the biological safety cabinet at room temperature, and imaged with a scanning electron microscope (JSM-7500F; Jeol

USA, Peabody, MA, USA) for visualizing the cell surface. Before SEM imaging, 5 nm palladium and platinum (Pd/Pt) alloys were deposited on the surfaces to ensure the electrical conductivity for SEM measurements and to immobilize adhered bacteria cells.

2.4. Characterization of MoS₂

The morphology and size characteristics of bulk MoS₂ and MoS₂ nanosheets were determined using scanning electron microscopy (SEM) and atomic force microscopy (AFM). In both cases, after MoS₂ nanosheet stock solution was diluted 100-fold in DI water, a droplet of suspension was placed on a (100) silicon wafer, followed by 24 h drying at room temperature. The samples were characterized with an atomic force microscope (AFM, Bruker Dimension Icon, Billerica, MA, USA) using the tapping mode at room temperature in standard air atmosphere. The measurements were performed with a silicon tip (OMCL-AC200TS-R3, Olympus, Center Valley, PA, USA) which had a radius of curvature of 7 nm, a spring constant of 9 N/m, and a resonant frequency of 150 kHz, at a scan rate of 0.5 Hz. SEM measurements of MoS₂ samples were carried out similarly to the SEM characterization of bacteria, although no conductive layer was used for the MoS₂ samples.

The pH of MoS₂ suspension in water assisted by magnetic bar stirring was measured with a pH meter (S20 SevenEasy pH, Mettler Toledo, Columbus, OH, USA). The pH measurements were carried out as a function of suspension age (initial, 2 h, 4 h, 8 h, 12 h, and 24 h) and concentration (1.6 mg/mL, 4.0 mg/mL, 8.0 mg/mL, 16.0 mg/mL) for both bulk MoS₂ and nanoexfoliated MoS₂. All measurements were repeated at least three different times from different batches of samples to enable statistical analysis to be performed.

2.5. Zeta Potential Measurements

The zeta potential of the samples, which is the potential at the slipping/shear plane of colloid particle movement assisted by electric field energy [51], was measured with a dynamic light scattering (DLS) instrument (Malvern Instruments, Ltd., Malvern, UK) at 25 °C. The zeta potential was calculated from the Helmholtz–Smoluchowski equation using the electrophoretic mobility, dynamic viscosity of the continuous phase, and dielectric permittivity factor at the liquid and vacuum of the continuous phase [51,52]. All colloidal entities (bulk MoS₂, exfoliated MoS₂, *Bacillus cereus*, and *Pseudomonas aeruginosa*) were diluted to a lower concentration of 0.1 vol% to 1 vol% for the zeta potential measurements.

2.6. Analysis of MoS₂ Toxicity and Dose–Response Analysis

To observe overall survivability trends, two different soil bacteria were inoculated with bulk and exfoliated MoS₂ at five different concentrations (0, 1.6, 4.0, 8.0, and 16.0 mg/mL) and six different time points (0 h, 2 h, 4 h, 8 h, 12 h, and 24 h). A transfer of 1 mL was taken from samples which were incubated with the mixture of peptone water and MoS₂ suspension with a stirring magnetic bar for a pre-defined period of exposure time. Then, the 1 mL mixture was filled with warm TSA (40 °C) in a new Petri dish and gently shaken. Upon solidification for 10 min, the samples were placed in an aerobic incubation chamber at 37 °C for 24 h. Experiments were conducted at least in triplicates (up to seven repeats) for each concentration and time condition. The number of grown colonies after 24 h was counted from the TSA Petri dish by multiplying its dilution rate. The bacterial survival numbers, N , were normalized based on the initial colony number, N_0 , for each treatment (Equation (1)).

$$N_{\text{normalized survival}} = \frac{N}{N_0} \quad (1)$$

Dose–response curves were analyzed using a Sigmoidal model, as shown in Equation (2), with the aid of Origin software (Origin Pro 8, OriginLab Corp., Northampton, MA, USA).

$$y = \min + \frac{\max - \min}{(1 + 10^{\text{LogEC}_{50} - X})} \quad (2)$$

where X is the logarithm of MoS_2 concentration, min is the bacterial survival number at the bottom plateau, and max is the bacterial survival number at the top plateau.

2.7. Statistical Analysis

To obtain the average and standard deviations, the statistical package in Analysis ToolPak-Excel (Microsoft Corp., Redmond, WA, USA) was used. For comparing the statistical differences in the survivability of *B. cereus* and *P. aeruginosa*, two-way analysis of variance (ANOVA) with Tukey's post hoc test was utilized to determine the statistical similarity of the data sets with p -values.

3. Results and Discussion

3.1. Characterization of Soil Bacteria

In many physicochemically interacting systems, the interplay among relevant characteristic length scales such as particle size, particle thickness, bacterial diameter, and bacterial size often controls the dynamics of interactions. Accordingly, we first investigated the morphological characteristics of soil bacteria. Figure 1a,b shows SEM micrographs of *B. cereus* and *P. aeruginosa* in the absence of any exposure to MoS_2 . The average size of *B. cereus* was slightly larger than that of *P. aeruginosa* for both length and the diameter described in Table 1. The average length and diameter of *B. cereus* was $2.86 \pm 0.83 \mu\text{m}$ and $0.79 \pm 0.10 \mu\text{m}$, respectively; the average length and diameter of *P. aeruginosa* was $2.31 \pm 0.41 \mu\text{m}$ and $0.63 \pm 0.18 \mu\text{m}$. Furthermore, extracellular polymeric substances (EPS) excreted by bacteria, which contain polysaccharides, proteins, nucleic acids, lipids, and other macromolecules to assist the adaptation of the cells by making them attach and aggregate on the surfaces [53,54], could also be seen from these SEM micrographs.

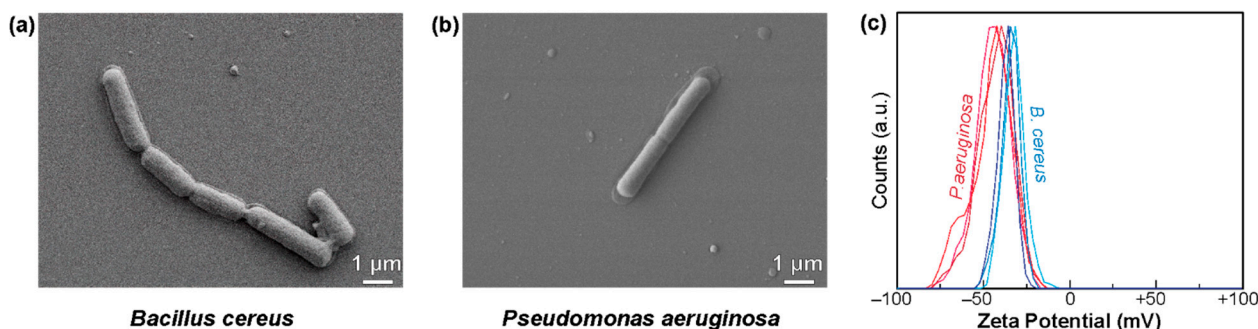


Figure 1. Scanning electron microscopy images of (a) *B. cereus* and (b) *P. aeruginosa*, and (c) zeta-potential of these microorganisms.

Table 1. The structural and surface characteristics of *B. cereus* and *P. aeruginosa* used in this study. \pm values indicate the standard deviation.

Bacteria	<i>B. cereus</i>	<i>P. aeruginosa</i>
Type	Gram-positive	Gram-negative
Dimensions (μm)	W: 0.79 ± 0.10 L: 2.86 ± 0.83	W: 0.63 ± 0.18 L: 2.31 ± 0.41
Zeta potential (mV)	-33.3 ± 1.1	-44.3 ± 1.2

Zeta potential value is an important parameter that controls the interfacial behavior of bacteria such as the colloidal stability and adhesion [55,56]. Figure 1c indicates the zeta potential of *B. cereus* and *P. aeruginosa* in DI water. *B. cereus* has a zeta-potential of $-33.3 \pm 1.1 \text{ mV}$, whereas *P. aeruginosa* has a zeta potential of $-44.3 \pm 1.2 \text{ mV}$. These values are sufficiently large that colloidal aggregation of these bacteria is unlikely to occur. The differences in the zeta potential can be attributed to the differences in Gram-positive and Gram-negative bacterial walls. Gram-positive bacteria are negatively charged due to the presence of teichoic acid containing glycerol or ribitol phosphates which can contribute to

the antibiotic susceptibility of bacteria [57,58]. On the other hand, Gram-negative bacteria are negatively charged because of the presence of lipopolysaccharides, which provide them with their adhesive ability for survival and stabilizing their outer membrane to protect the inner structure [59,60].

3.2. Characterization of MoS₂

Comparison of size characteristics of MoS₂ with bacteria is important to gain insights into the relative mobility of MoS₂ and bacteria in aqueous media and the surface potential of MoS₂ to cover bacteria surfaces. Figure 2 demonstrates micrographs of bulk MoS₂ and MoS₂ nanosheets as well as their zeta potentials. Image analysis over multiple samples (summarized in Table 2) revealed that bulk MoS₂ has a mean diameter of $12.0 \pm 7.6 \mu\text{m}$ (geometric mean) and a thickness of $520 \pm 364 \text{ nm}$. On the other hand, the diameter and thickness of MoS₂ nanosheets were $0.88 \pm 0.81 \mu\text{m}$ and $3.1 \pm 0.7 \text{ nm}$, respectively. These size characteristics indicated that the ultrasonication process not only separated the layers, but also broke the layers into smaller fragments in the planar direction. In the existing literature, nanomaterials with a thickness of less than 1–10 nm, as in the case of exfoliated MoS₂ in this study, are often categorized as 2D nanosheets [31,61]. Given that the thickness of each MoS₂ layer is reported to be 0.65 nm [62], a thickness of 2 to 4 nm corresponds to three to six layers.

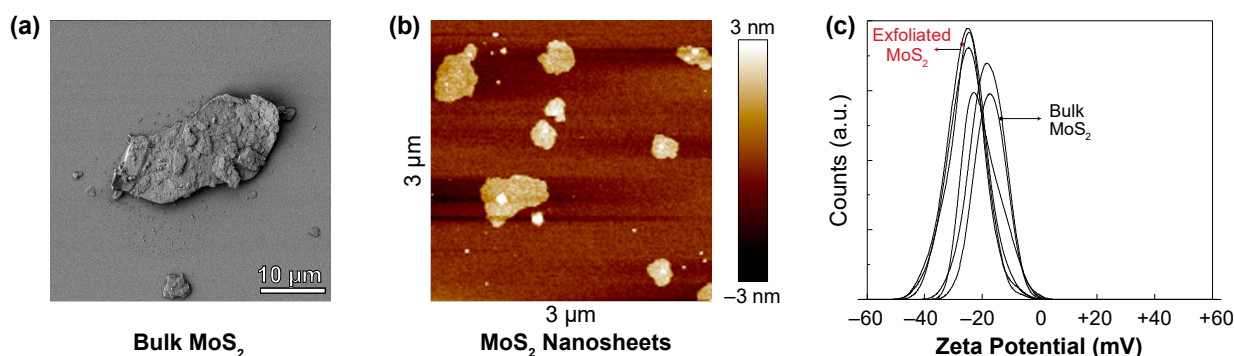


Figure 2. (a) Scanning electron microscopy image of bulk MoS₂, (b) atomic force microscopy image of 2D MoS₂ nanosheets, and (c) zeta potential of bulk and exfoliated MoS₂.

Table 2. The structural and surface characteristics of bulk and exfoliated MoS₂ used in this study.

MoS ₂	Bulk Form	Exfoliated Form
Planar diameter (μm)	12.0 ± 7.6	0.9 ± 0.8
Thickness (nm)	520 ± 364	3.1 ± 0.7
Zeta potential (mV)	-18.4 ± 1.5	-25.4 ± 0.2

\pm values indicate the standard deviation.

As can be seen from Figure 2c, zeta potential values of $-18.4 \pm 1.5 \text{ mV}$ and $-25.4 \pm 0.2 \text{ mV}$ were observed for bulk MoS₂ and exfoliated MoS₂, respectively. Accordingly, the electrostatic interactions between MoS₂ and bacteria are repulsive. For the case of interactions between MoS₂ particles and bacteria in water, even if the overall interaction electrical charge between bacteria and MoS₂ is repulsive, there is a Boltzmann probability of MoS₂ adhesion on bacteria (or bacterial adhesion on MoS₂) governed by the magnitude of the activation energy in terms of kT [63,64]. Furthermore, prior studies have indicated that nanosheets can orient themselves perpendicularly to the surfaces during the approach to significantly reduce the magnitude of repulsion [14]. For instance, the deposition of negatively charged graphene oxide on self-assembled monolayers of 6-aminohexylaminopropyltrimethoxysilane, which possess a negative zeta potential above pH ~ 6 , was confirmed via AFM studies [14,65,66].

3.3. Survival of *B. cereus* and *P. aeruginosa* against MoS₂ Exposure

As can be seen from Figure 3, the addition of MoS₂ into *B. cereus* suspension resulted in a concentration-dependent reduction in bacterial survival. For the case of bulk MoS₂ exposure, the survival data followed an initially rapidly decreasing trend, which gradually plateaued out after an exposure time of 8 h. The log reduction in survival upon 24 h exposure was ~0.3 (55% reduction) and ~2.6 (99.7% reduction) at a MoS₂ concentration of 1.6 mg/mL and 16.0 mg/mL, respectively. For the case of exfoliated MoS₂, similar trends were also observed, but the log-reductions in survival numbers were much larger: ~0.9 (86% reduction) at 1.6 mg/mL and ~4.9 (99.999% reduction) at 16.0 mg/mL.

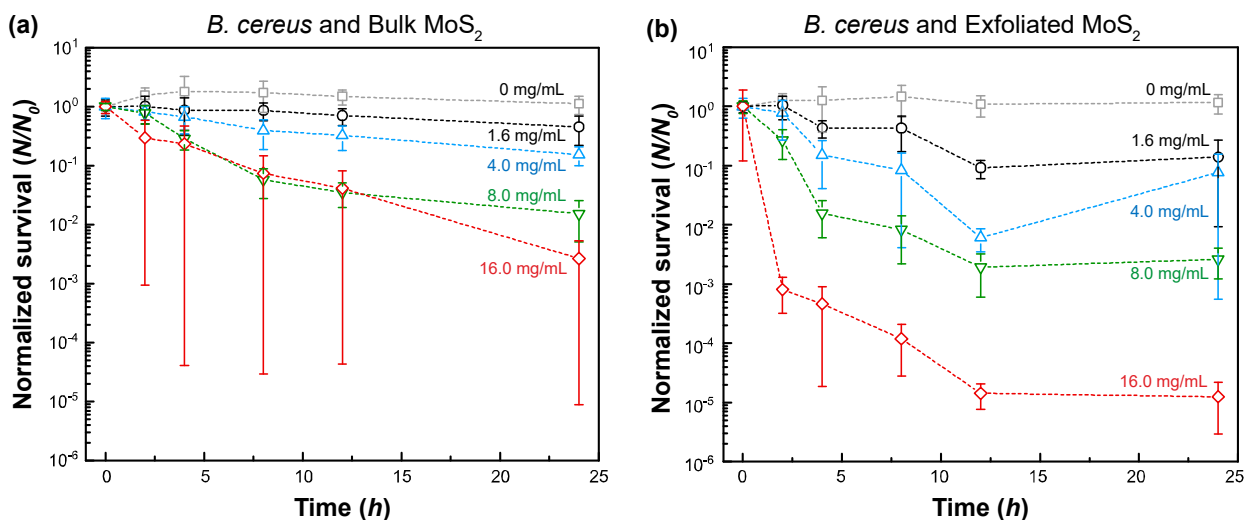


Figure 3. Normalized (with respect to initial concentration) survival of *B. cereus* in peptone water and MoS₂ suspension inoculated with (a) bulk MoS₂ and (b) exfoliated MoS₂. The error bars represent the standard error of the mean.

Similar to the studies with Gram-positive *B. cereus*, the influence of MoS₂ on the survival of Gram-negative *P. aeruginosa* was also investigated (Figure 4). At a concentration of 16.0 mg/mL, the log-reduction in bacterial survival was ~1.9 (98.6%) and ~5.5 (99.9997%) for bulk MoS₂ and exfoliated MoS₂, respectively. Overall, *P. aeruginosa* demonstrated a slightly higher survival rate than *B. cereus* against bulk MoS₂, whereas exfoliated MoS₂, above a concentration of 1.6 mg/mL, resulted in the lower survival of *P. aeruginosa* compared to *B. cereus*.

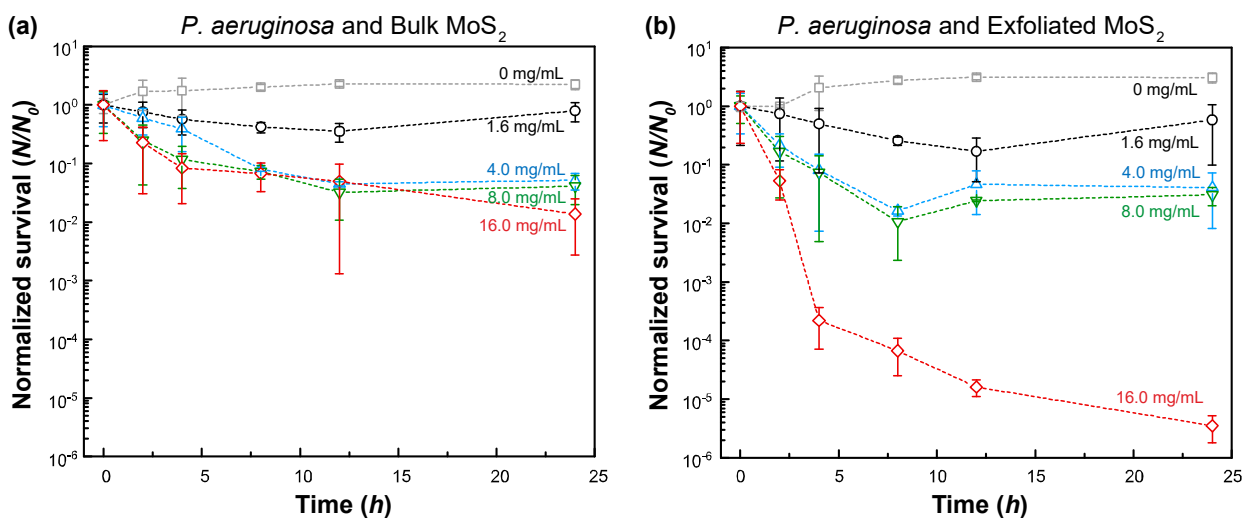


Figure 4. Normalized (with respect to initial concentration) survival of *P. aeruginosa* in peptone water and MoS₂ suspension inoculated with (a) bulk MoS₂ and (b) exfoliated MoS₂. The error bars represent the standard error of the mean.

Based on the statistical analysis, the toxicity levels of bulk MoS₂ and exfoliated MoS₂ were found to be statistically different for both bacteria ($p < 0.05$, see the Supplementary Materials for further details: Table S2a). In addition, the toxicity of exfoliated MoS₂ was always higher than bulk MoS₂ (see the Supplementary Materials for further details, Table S2b).

The gradually plateauing trends observed in these cases can be attributed to the following possibilities. First, given that a predefined amount of MoS₂ exists in the suspension, continuous adsorption/uptake of MoS₂ on/in bacteria gradually reduces the MoS₂ concentration in the suspension. As new bacteria grow, the effective concentration of MoS₂ becomes less and less with time. This could explain the plateauing trend and trends that the survival increases at a sufficiently long time. Secondly, the presence of bacteria and excreted extracellular polymeric substances (EPS) can induce the aggregation of MoS₂ and the encapsulation/coverage of MoS₂ with the EPS layer, which can reduce the surface dissociation processes and effective solubilization (i.e., bioavailability). Similarly, chemical changes can also take place on MoS₂ in the presence of EPS. These effects, in turn, can reduce the potency of MoS₂ as a toxic agent to bacteria.

Based on the analysis of the data shown in Figures 3 and 4, a dose–response curve was constructed for bulk MoS₂ control and exfoliated MoS₂ (Figure 5 and Table S3). The response curve relied on 8 h data as the suspension seemed to be depleted/sedimented for longer durations. It was found that the median effective concentration (EC₅₀) was 1.81 ± 0.41 mg/mL and 1.00 ± 0.43 mg/mL for the case of bulk MoS₂ against *B. cereus* and *P. aeruginosa*, respectively. On the other hand, for the case of MoS₂ nanosheets, EC₅₀ values of 1.45 ± 0.19 mg/mL and 0.59 ± 0.16 mg/mL were obtained *B. cereus* and *P. aeruginosa*, respectively. By comparing the median minimum bactericidal concentrations (MBC₅₀) for other antimicrobial agents from the literature, such as clindamycin (1.0 µg/mL), gentamicin (2.0 µg/mL), vancomycin (2.0 µg/mL) for *B. cereus* [67], and ceftazidime (128.0 µg/mL), tobramycin (16.0 µg/mL), meropenem (16.0 µg/mL), aztreonam (128.0 µg/mL), piperacillin (64.0 µg/mL) for *P. aeruginosa* [68], it can be stated that EC₅₀ values of bulk and exfoliated MoS₂ are one to three orders of magnitude higher, indicating the relatively weak bacterial toxicity of MoS₂. However, at sufficiently high concentrations (>~1 mg/mL), bulk and nanoexfoliated MoS₂ can moderately inhibit the growth of *B. cereus* and *P. aeruginosa*.

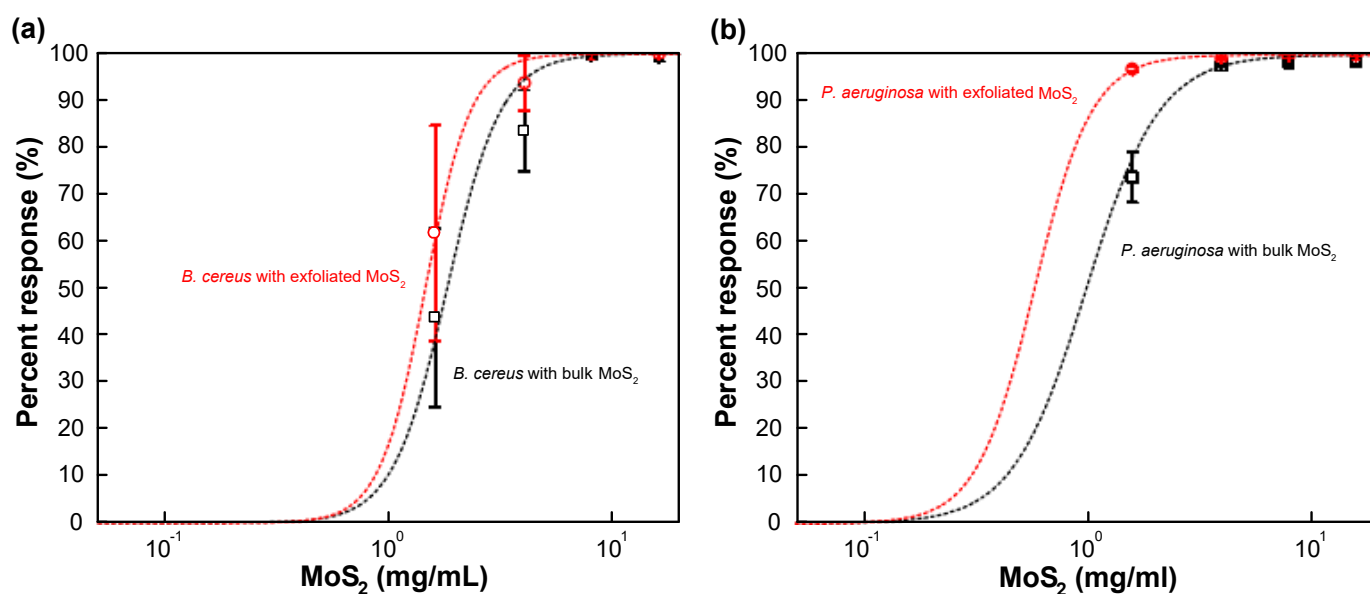


Figure 5. Dose–response curve of (a) *B. cereus* and (b) *P. aeruginosa* against bulk and exfoliated MoS₂. The error bars represent the standard error of the mean.

3.4. Mechanism of Interaction between MoS₂ and Bacteria

To gain a mechanistic understanding of how MoS₂ interacts with and inactivates bacteria, SEM studies were performed (Figure 6, Figures S4 and S5). It was found that bulk MoS₂ acts as a geometrical obstacle that hinders the formation of bacterial microcolonies and confines bacteria. In the presence of bulk MoS₂, no significant change in the morphology of bacteria was observed. On the other hand, exfoliated MoS₂ induced wrinkles and rhytids on a bacterial wall. Furthermore, due to its smaller size and thinner nature, exfoliated MoS₂ could better conform to the curvature of bacteria. The mean length of bacteria exposed to exfoliated MoS₂ was smaller than that exposed to bulk MoS₂ and no treatment.

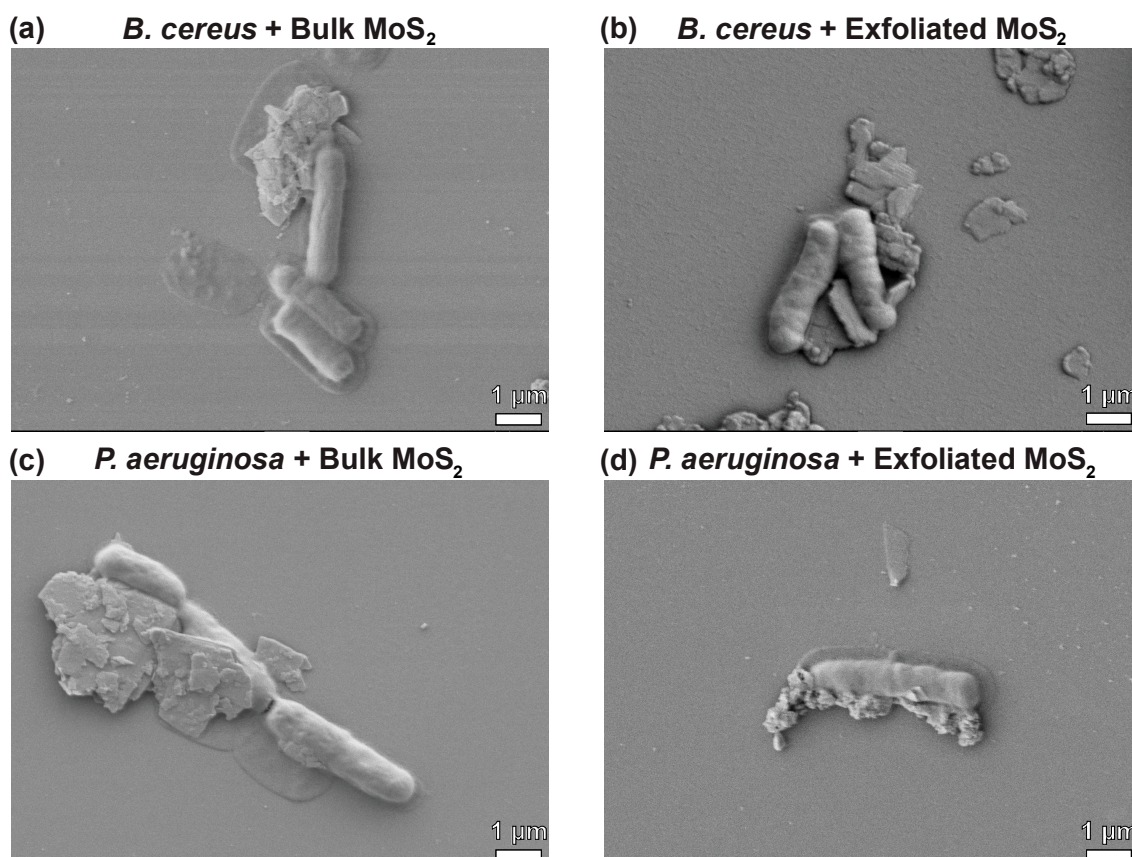
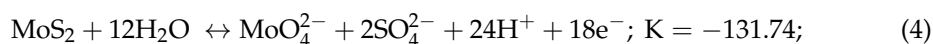
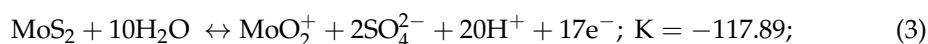


Figure 6. SEM micrographs showing interactions between soil bacteria and MoS₂ particles at a concentration of 4.0 mg/mL for an inoculation time of 12 h. (a) *B. cereus* inoculated with bulk MoS₂, (b) *B. cereus* inoculated with exfoliated MoS₂, (c) *P. aeruginosa* inoculated with bulk MoS₂, and (d) *P. aeruginosa* inoculated with exfoliated MoS₂. Additional SEM images are shown in Figures S5 and S6, in the Supplementary Materials.

The presence of oxidative stress, which can be induced by MoS₂ via the formation of oxides and sulfate ions [69,70] on the bacteria, could be the reason for wrinkles and rhytids on the cell. The local oxidation and etching/erosion of the cell wall can cause mechanical instabilities where the internal osmotic pressure can locally push thinner regions outward (i.e., nano-/micro-bulging) while the intact regions of the cell wall may remain mostly unaltered. Kaur et al. [56] observed the fragmentation and damage of cell walls for MCF7 (breast cancer), U937 (leukemia), HaCaT (epithelium), and *Salmonella typhimurium* upon inoculation with MoS₂ nanosheets at a concentration of 10–20 μg/mL. Pandit et al. [71] reported the antibacterial activity of quaternary amine-functionalized, chemically exfoliated MoS₂ nanosheets against *Staphylococcus aureus* and *Pseudomonas aeruginosa*, whereas hydroxyl-functionalized MoS₂ nanosheets showed no antibacterial activity. These findings suggest that ligands rather than MoS₂ play a larger role in antibacterial activity. In addition, each bacterium can exhibit a different favorable environmental condition, such

as mesophilic, thermophilic, acidophilic, and alkaliphilic conditions. Some bacteria can survive in oxidative stress conditions owing to their defensive systems [72]. *B. cereus* and *P. aeruginosa* are known to be mesophiles. However, *B. cereus* possesses gene clusters responsible for the arginine deiminase metabolic pathway, which is believed to play a pivotal role in resisting acidic conditions [73–75]. The range of pH allowing growth of *B. cereus* was reported to be pH 4.9 to 9.3 [76]. Based on acid treatment studies, Bushell et al. [77] reported that the growth rate of *P. aeruginosa* does not change much between pH 7 and 6, while noticeable reductions in bacterial growth are observed below pH 5.5, and almost no growth occurs at pH 5. Accordingly, we have also investigated the change in dispersion pH upon the addition of bulk and exfoliated MoS₂.

It was found that the presence of bulk MoS₂ reduced the dispersion pH to 6.3 and 4.3 at concentrations of 1.6 mg/mL and 16.0 mg/mL, respectively (Figure S6, Supplementary Materials). In contrast, dispersion pH values of 5.4 and 3.5 were attained for the case of MoS₂ nanosheets at concentrations of 1.6 mg/mL and 16.0 mg/mL, respectively, indicating a more acidifying potential of exfoliated MoS₂. Two potential dissociating processes of MoS₂, one involving a 1:10 MoS₂:H₂O ratio and another involving a 1:12 MoS₂:H₂O ratio, were described by Titley et al. [78] and Wagman et al. [79] with dissociation equilibrium constants of −117.89 and −131.74, as shown in Equations (3) and (4).



In addition, sulfur atoms of MoS₂ can be replaced by oxygen atoms via oxidation when kept in aqueous media for prolonged periods of time [69]. Liu et al. [80] reported that MoO₂ has two kinds of proton-donating ligands, with pK_a values of 4.7 (OH) and 10.6 (H₂O) from MoO₂(OH)₂·(H₂O)₂, which indicates that even after the transformation from MoS₂, molybdenum oxides would persist in having an acidic nature. When plotted as growth trends, we can see that the higher concentrations of MoS₂ give rise to environments that are unfavorable for the soil bacteria studied in this work. This means that apart from oxidative stress and blockage of the cell wall, acidity induced by the presence of MoS₂ should also be considered in the context of toxicity of MoS₂.

4. Conclusions

Two-dimensional nanosheets are important types of emerging nanomaterials receiving attention from various fields and applications. In this study, we investigated the toxicity of 2D MoS₂ nanosheets (nanoscale) on soil bacteria *B. cereus* and *P. aeruginosa* and compared it with bulk MoS₂ (macroscale) at various concentrations. It was found that 2D MoS₂ nanosheets demonstrate a higher level of toxicity against these microorganisms than bulk MoS₂. The 8 h EC₅₀ value was 1.81 ± 0.41 mg/mL and 1.00 ± 0.43 mg/mL for bulk MoS₂ against *B. cereus* and *P. aeruginosa*, respectively. In contrast, for exfoliated MoS₂ nanosheets, EC₅₀ values of 1.45 ± 0.19 mg/mL and 0.59 ± 0.16 mg/mL were obtained for *B. cereus* and *P. aeruginosa*, respectively. Three potential mechanisms of action have been identified as oxidative stress: the coverage and blockage of cell walls of nanosheets, the dissolution of MoS₂, and the resulting acidification of the dispersion medium. Oxidative stress and acidification induced wrinkles and rhytids on bacterial walls. The blockage of cell walls, which was confirmed with SEM studies, can hinder nutrient transport and metabolic activities that occur on the cell wall. Compared to antimicrobial agents such as clindamycin, gentamicin, vancomycin, tobramycin, and piperacillin, EC₅₀ values of bulk and exfoliated MoS₂ are one to three orders of magnitude higher, indicating the relatively weak bacterial toxicity of MoS₂. Overall, this study highlights the potential of MoS₂ nanotoxicity on beneficial soil bacteria, which plays an essential role in nitrate reduction and nitrogen fixation, soil formation, the decomposition of dead and decayed natural materials, and the transformation of toxic compounds into nontoxic compounds.

Supplementary Materials: The following are available online at <https://www.mdpi.com/article/10.3390/nano11061453/s1>, Figure S1: Digital photo of MoS₂ nanosheets in water, Figure S2: Size data of MoS₂ nanosheets in water, Figure S3: Schematic protocol for preparing plate counting samples, Figures S4 and S5: Additional SEM micrographs for bacteria interactions with MoS₂, Figure S6: pH plot corresponding to survival results, Table S1: Starting material (MoS₂) information, Table S2: Statistical data obtained from survival results, Table S3: Fitting data from the dose–response curve.

Author Contributions: The manuscript was written through contributions of all authors. Both authors M.B. and J.K.O. contributed equally to this work. S.L., N.N., Y.Y., W.D. have assisted the data acquisition and curation. L.C.-Z. and E.M.A.S. have supervised this work. All authors have read and agreed to the published version of the manuscript.

Funding: This work is partly supported by the Food Manufacturing Technologies Program, A1363; Grant No. 2019-68015-29231; Project Accession No. TEX09762, from the USDA National Institute of Food and Agriculture. Part of this work was supported by the Energy Institute Master of Science Program to M.B. and E.M.A.S. [81]. This work was also partly supported by NSF Award # 1236532.

Acknowledgments: The preparation of bacteria was supported by students (Tamra Tolen and Samuel Annor) from Taylor’s group.

Conflicts of Interest: The authors declare no conflict of interest.

References

1. Arvidsson, R.; Baun, A.; Furberg, A.; Hansen, S.F.; Molander, S. Proxy measures for simplified environmental assessment of manufactured nanomaterials. *Environ. Sci. Technol.* **2018**, *52*, 13670–13680. [[CrossRef](#)] [[PubMed](#)]
2. Pagano, L.; Servin, A.D.; De La Torre-Roche, R.; Mukherjee, A.; Majumdar, S.; Hawthorne, J.; Marmioli, M.; Maestri, E.; Marra, R.E.; Isch, S.M. Molecular response of crop plants to engineered nanomaterials. *Environ. Sci. Technol.* **2016**, *50*, 7198–7207. [[CrossRef](#)]
3. Oh, J.K.; Liu, S.; Jones, M.; Yegin, Y.; Hao, L.; Tolen, T.N.; Nagabandi, N.; Scholar, E.A.; Castillo, A.; Taylor, T.M.; et al. Modification of aluminum surfaces with superhydrophobic nanotextures for enhanced food safety and hygiene. *Food Control* **2019**, *96*, 463–469. [[CrossRef](#)]
4. Sakimoto, K.K.; Kornienko, N.; Cestellos-Blanco, S.; Lim, J.; Liu, C.; Yang, P. Physical biology of the materials–microorganism interface. *J. Am. Chem. Soc.* **2018**, *140*, 1978–1985. [[CrossRef](#)]
5. Dimkpa, C.O.; McLean, J.E.; Latta, D.E.; Manangón, E.; Britt, D.W.; Johnson, W.P.; Boyanov, M.I.; Anderson, A.J. CuO and ZnO nanoparticles: Phytotoxicity, metal speciation, and induction of oxidative stress in sand-grown wheat. *J. Nanopart. Res.* **2012**, *14*, 1125. [[CrossRef](#)]
6. Xin, Q.; Rotchell, J.M.; Cheng, J.; Yi, J.; Zhang, Q. Silver nanoparticles affect the neural development of zebrafish embryos. *J. Appl. Toxicol.* **2015**, *35*, 1481–1492. [[CrossRef](#)]
7. Liu, S.; Zeng, T.H.; Hofmann, M.; Burcombe, E.; Wei, J.; Jiang, R.; Kong, J.; Chen, Y. Antibacterial activity of graphite, graphite oxide, graphene oxide, and reduced graphene oxide: Membrane and oxidative stress. *ACS Nano* **2011**, *5*, 6971–6980. [[CrossRef](#)]
8. Zhang, D.; Yao, Y.; Duan, Y.; Yu, X.; Shi, H.; Nakkala, J.R.; Zuo, X.; Hong, L.; Mao, Z.; Gao, C. Surface-Anchored Graphene Oxide Nanosheets on Cell-Scale Micropatterned Poly(d, l-lactide- co-caprolactone) Conduits Promote Peripheral Nerve Regeneration. *ACS Appl. Mater. Interfaces* **2020**. [[CrossRef](#)]
9. He, X.; Aker, W.G.; Fu, P.P.; Hwang, H.M. Toxicity of engineered metal oxide nanomaterials mediated by nano-bio-eco-interactions: A review and perspective. *Environ. Sci. Nano* **2015**, *2*, 564–582. [[CrossRef](#)]
10. Sasidharan, A.; Panchakarla, L.S.; Chandran, P.; Menon, D.; Nair, S.; Rao, C.N.R.; Koyakutty, M. Differential nano-bio interactions and toxicity effects of pristine versus functionalized graphene. *Nanoscale* **2011**, *3*, 2461–2464. [[CrossRef](#)] [[PubMed](#)]
11. Liu, S.; Bae, M.; Hao, L.; Oh, J.K.; White, A.R.; Min, Y.; Cisneros-Zevallos, L.; Akbulut, M. Bacterial antifouling characteristics of helicene—Graphene films. *Nanomaterials* **2021**, *11*, 89. [[CrossRef](#)]
12. Agarwal, V.; Chatterjee, K. Recent advances in the field of transition metal dichalcogenides for biomedical applications. *Nanoscale* **2018**, *10*, 16365–16397. [[CrossRef](#)]
13. Hantanasirisakul, K.; Gogotsi, Y. Electronic and Optical Properties of 2D Transition Metal Carbides and Nitrides (MXenes). *Adv. Mater.* **2018**, *30*, 1–30. [[CrossRef](#)]
14. Chen, I.C.; Zhang, M.; Min, Y.; Akbulut, M. Deposition Kinetics of Graphene Oxide on Charged Self-Assembled Monolayers. *J. Phys. Chem. C* **2016**, *120*, 8333–8342. [[CrossRef](#)]
15. Yegin, C.; Nagabandi, N.; Feng, X.; King, C.; Catalano, M.; Oh, J.K.; Talib, A.J.; Scholar, E.A.; Verkhoturov, S.V.; Cagin, T.; et al. Metal-Organic-Inorganic Nanocomposite Thermal Interface Materials with Ultralow Thermal Resistances. *ACS Appl. Mater. Interfaces* **2017**, *9*. [[CrossRef](#)]
16. Wu, D.; Bai, Y.; Wang, W.; Xia, H.; Tan, F.; Zhang, S.; Su, B.; Wang, X.; Qiao, X.; Wong, P.K. Highly pure MgO₂ nanoparticles as robust solid oxidant for enhanced Fenton-like degradation of organic contaminants. *J. Hazard. Mater.* **2019**, *374*, 319–328. [[CrossRef](#)]

17. David, L.; Bhandavat, R.; Singh, G. MoS₂/graphene composite paper for sodium-ion battery electrodes. *ACS Nano* **2014**, *8*, 1759–1770. [[CrossRef](#)] [[PubMed](#)]
18. Sgroi, M.F.; Asti, M.; Gili, F.; Deorsola, F.A.; Bensaid, S.; Fino, D.; Kraft, G.; Garcia, I.; Dassenoy, F. Engine bench and road testing of an engine oil containing MoS₂ particles as nano-additive for friction reduction. *Tribol. Int.* **2017**, *105*, 317–325. [[CrossRef](#)]
19. Li, W.; Geng, X.; Guo, Y.; Rong, J.; Gong, Y.; Wu, L.; Zhang, X.; Li, P.; Xu, J.; Cheng, G. Reduced graphene oxide electrically contacted graphene sensor for highly sensitive nitric oxide detection. *ACS Nano* **2011**, *5*, 6955–6961. [[CrossRef](#)] [[PubMed](#)]
20. Tian, Z.; Mahurin, S.M.; Dai, S.; Jiang, D. Ion-gated gas separation through porous graphene. *Nano Lett.* **2017**, *17*, 1802–1807. [[CrossRef](#)]
21. Dervin, S.; Dionysiou, D.D.; Pillai, S.C. 2D nanostructures for water purification: Graphene and beyond. *Nanoscale* **2016**, *8*, 15115–15131. [[CrossRef](#)]
22. Zhao, N.; Yang, M.; Zhao, Q.; Gao, W.; Xie, T.; Bai, H. Superstretchable nacre-mimetic graphene/poly (vinyl alcohol) composite film based on interfacial architectural engineering. *ACS Nano* **2017**, *11*, 4777–4784. [[CrossRef](#)]
23. Hao, L.; Chen, I.-C.; Oh, J.K.; Nagabandi, N.; Bassan, F.; Liu, S.; Scholar, E.; Zhang, L.; Akbulut, M.; Jiang, B. Nanocomposite Foam Involving Boron Nitride Nanoplatelets and Polycaprolactone: Porous Structures with Multiple Length Scales for Oil Spill Cleanup. *Ind. Eng. Chem. Res.* **2017**, *56*. [[CrossRef](#)]
24. Su, Y.; Tong, X.; Huang, C.; Chen, J.; Liu, S.; Gao, S.; Mao, L.; Xing, B. Green algae as carriers enhance the bioavailability of ¹⁴C-labeled few-layer graphene to freshwater snails. *Environ. Sci. Technol.* **2018**, *52*, 1591–1601. [[CrossRef](#)]
25. Kang, W.; Li, X.; Sun, A.; Yu, F.; Hu, X. Study of the persistence of the phytotoxicity induced by graphene oxide quantum dots and of the specific molecular mechanisms by integrating omics and regular analyses. *Environ. Sci. Technol.* **2019**, *53*, 3791–3801. [[CrossRef](#)] [[PubMed](#)]
26. Li, Y.; Jin, Q.; Yang, D.; Cui, J. Molybdenum sulfide induce growth enhancement effect of rice (*Oryza sativa* L.) through regulating the synthesis of chlorophyll and the expression of aquaporin gene. *J. Agric. Food Chem.* **2018**, *66*, 4013–4021. [[CrossRef](#)] [[PubMed](#)]
27. Ataca, C.; Ciraci, S. Functionalization of single-layer MoS₂ honeycomb structures. *J. Phys. Chem. C* **2011**, *115*, 13303–13311. [[CrossRef](#)]
28. Li, H.; Wu, J.; Yin, Z.; Zhang, H. Preparation and applications of mechanically exfoliated single-layer and multilayer MoS₂ and WSe₂ nanosheets. *Acc. Chem. Res.* **2014**, *47*, 1067–1075. [[CrossRef](#)]
29. Wu, J.; Li, H.; Yin, Z.; Li, H.; Liu, J.; Cao, X.; Zhang, Q.; Zhang, H. Layer thinning and etching of mechanically exfoliated MoS₂ nanosheets by thermal annealing in air. *Small* **2013**, *9*, 3314–3319. [[CrossRef](#)]
30. Lukowski, M.A.; Daniel, A.S.; Meng, F.; Forticaux, A.; Li, L.; Jin, S. Enhanced hydrogen evolution catalysis from chemically exfoliated metallic MoS₂ nanosheets. *J. Am. Chem. Soc.* **2013**, *135*, 10274–10277. [[CrossRef](#)] [[PubMed](#)]
31. Rowley-Neale, S.J.; Brownson, D.A.C.; Smith, G.C.; Sawtell, D.A.G.; Kelly, P.J.; Banks, C.E. 2D nanosheet molybdenum disulphide (MoS₂) modified electrodes explored towards the hydrogen evolution reaction. *Nanoscale* **2015**, *7*, 18152–18168. [[CrossRef](#)]
32. Paul, J.F.; Payen, E. Vacancy formation on MoS₂ hydrodesulfurization catalyst: DFT study of the mechanism. *J. Phys. Chem. B* **2003**, *107*, 4057–4064. [[CrossRef](#)]
33. Garadkar, K.M.; Patil, A.A.; Hankare, P.P.; Chate, P.A.; Sathe, D.J.; Delekar, S.D. MoS₂: Preparation and their characterization. *J. Alloy. Compd.* **2009**, *487*, 786–789. [[CrossRef](#)]
34. Conley, H.J.; Wang, B.; Ziegler, J.I.; Haglund, R.F.; Pantelides, S.T.; Bolotin, K.I. Bandgap engineering of strained monolayer and bilayer MoS₂. *Nano Lett.* **2013**, *13*, 3626–3630. [[CrossRef](#)]
35. Liu, C.; Kong, D.; Hsu, P.C.; Yuan, H.; Lee, H.W.; Liu, Y.; Wang, H.; Wang, S.; Yan, K.; Lin, D.; et al. Rapid water disinfection using vertically aligned MoS₂ nanofilms and visible light. *Nat. Nanotechnol.* **2016**, *11*, 1098–1104. [[CrossRef](#)] [[PubMed](#)]
36. Amin, M.; Rowley-Neale, S.; Shalamanova, L.; Lynch, S.; Wilson-Nieuwenhuis, J.T.; El Mohtadi, M.; Banks, C.E.; Whitehead, K.A. Molybdenum Disulfide Surfaces to Reduce *Staphylococcus aureus* and *Pseudomonas aeruginosa* Biofilm Formation. *ACS Appl. Mater. Interfaces* **2020**, *12*, 21057–21069. [[CrossRef](#)]
37. Delgado-Baquerizo, M.; Oliverio, A.M.; Brewer, T.E.; Benavent-González, A.; Eldridge, D.J.; Bardgett, R.D.; Maestre, F.T.; Singh, B.K.; Fierer, N. A global atlas of the dominant bacteria found in soil. *Science* **2018**, *359*, 320–325. [[CrossRef](#)] [[PubMed](#)]
38. Levenfors, J.J.; Hedman, R.; Thaning, C.; Gerhardson, B.; Welch, C.J. Broad-spectrum antifungal metabolites produced by the soil bacterium *Serratia plymuthica* A 153. *Soil Biol. Biochem.* **2004**, *36*, 677–685. [[CrossRef](#)]
39. Zouboulis, A.I.; Loukidou, M.X.; Matis, K.A. Biosorption of toxic metals from aqueous solutions by bacteria strains isolated from metal-polluted soils. *Process Biochem.* **2004**, *39*, 909–916. [[CrossRef](#)]
40. Dixit, R.; Wasiullah; Malaviya, D.; Pandiyan, K.; Singh, U.B.; Sahu, A.; Shukla, R.; Singh, B.P.; Rai, J.P.; Sharma, P.K.; et al. Bioremediation of heavy metals from soil and aquatic environment: An overview of principles and criteria of fundamental processes. *Sustainability* **2015**, *7*, 2189–2212. [[CrossRef](#)]
41. Hwang, G.; Ahn, I.-S.; Mhin, B.J.; Kim, J.-Y. Adhesion of nano-sized particles to the surface of bacteria: Mechanistic study with the extended DLVO theory. *Colloids Surf. B Biointerfaces* **2012**, *97*, 138–144. [[CrossRef](#)]
42. Rousk, J.; Ackermann, K.; Curling, S.F.; Jones, D.L. Comparative toxicity of nanoparticulate CuO and ZnO to soil bacterial communities. *PLoS ONE* **2012**, *7*, e34197. [[CrossRef](#)]
43. Hernandez-Viezas, J.A.; Castillo-Michel, H.; Andrews, J.C.; Cotte, M.; Rico, C.; Peralta-Videa, J.R.; Ge, Y.; Priester, J.H.; Holden, P.A.; Gardea-Torresdey, J.L. In situ synchrotron X-ray fluorescence mapping and speciation of CeO₂ and ZnO nanoparticles in soil cultivated soybean (*Glycine max*). *ACS Nano* **2013**, *7*, 1415–1423. [[CrossRef](#)] [[PubMed](#)]

44. Whiteside, M.D.; Treseder, K.K.; Atsatt, P.R. The brighter side of soils: Quantum dots track organic nitrogen through fungi and plants. *Ecology* **2009**, *90*, 100–108. [[CrossRef](#)] [[PubMed](#)]
45. Moll, J.; Gogos, A.; Bucheli, T.D.; Widmer, F.; Heijden, M.G.A. Effect of nanoparticles on red clover and its symbiotic microorganisms. *J. Nanobiotechnol.* **2016**, *14*, 36. [[CrossRef](#)] [[PubMed](#)]
46. Li, Y.; Chapman, S.J.; Nicol, G.W.; Yao, H. Nitrification and nitrifiers in acidic soils. *Soil Biol. Biochem.* **2018**, *116*, 290–301. [[CrossRef](#)]
47. Huang, F.; Wang, Z.-H.; Cai, Y.-X.; Chen, S.-H.; Tian, J.-H.; Cai, K.-Z. Heavy metal bioaccumulation and cation release by growing *Bacillus cereus* RC-1 under culture conditions. *Ecotoxicol. Environ. Saf.* **2018**, *157*, 216–226. [[CrossRef](#)]
48. Ayangbenro, A.S.; Babalola, O.O. Genomic analysis of *Bacillus cereus* NWUAB01 and its heavy metal removal from polluted soil. *Sci. Rep.* **2020**, *10*, 1–12. [[CrossRef](#)] [[PubMed](#)]
49. Hernandez, D.; Rowe, J.J. Oxygen regulation of nitrate uptake in denitrifying *Pseudomonas aeruginosa*. *Appl. Environ. Microbiol.* **1987**, *53*, 745–750. [[CrossRef](#)]
50. Ueno, A.; Hasanuzzaman, M.; Yumoto, I.; Okuyama, H. Verification of degradation of n-alkanes in diesel oil by *Pseudomonas aeruginosa* strain WatG in soil microcosms. *Curr. Microbiol.* **2006**, *52*, 182–185. [[CrossRef](#)]
51. Bhattacharjee, S. DLS and zeta potential—What they are and what they are not? *J. Control. Release* **2016**, *235*, 337–351. [[CrossRef](#)]
52. Předota, M.; Machesky, M.L.; Wesolowski, D.J. Molecular origins of the zeta potential. *Langmuir* **2016**, *32*, 10189–10198. [[CrossRef](#)]
53. Decho, A.W.; Gutierrez, T. Microbial extracellular polymeric substances (EPSs) in ocean systems. *Front. Microbiol.* **2017**, *8*, 1–28. [[CrossRef](#)]
54. Wingender, J. *Microbial Extracellular Polymeric Substances*; Springer: Berlin/Heidelberg, Germany, 1999; Volume 66, ISBN 9783642642777.
55. Boks, N.P.; Norde, W.; van der Mei, H.C.; Busscher, H.J. Forces involved in bacterial adhesion to hydrophilic and hydrophobic surfaces. *Microbiology* **2008**, *154*, 3122–3133. [[CrossRef](#)]
56. Kaur, J.; Singh, M.; Dell'Aversana, C.; Benedetti, R.; Giardina, P.; Rossi, M.; Valadan, M.; Vergara, A.; Cutarelli, A.; Montone, A.M.I.; et al. Biological interactions of biocompatible and water-dispersed MoS₂ nanosheets with bacteria and human cells. *Sci. Rep.* **2018**, *8*, 1–15. [[CrossRef](#)]
57. Swoboda, J.G.; Campbell, J.; Meredith, T.C.; Walker, S. Wall teichoic acid function, biosynthesis, and inhibition. *ChemBioChem* **2010**, *11*, 35–45. [[CrossRef](#)]
58. Xia, G.; Kohler, T.; Peschel, A. The wall teichoic acid and lipoteichoic acid polymers of *Staphylococcus aureus*. *Int. J. Med. Microbiol.* **2010**, *300*, 148–154. [[CrossRef](#)] [[PubMed](#)]
59. Valle, J.; Da Re, S.; Henry, M.; Fontaine, T.; Balestrino, D.; Latour-Lambert, P.; Ghigo, J.M. Broad-spectrum biofilm inhibition by a secreted bacterial polysaccharide. *Proc. Natl. Acad. Sci. USA* **2006**, *103*, 12558–12563. [[CrossRef](#)] [[PubMed](#)]
60. Foschiatti, M.; Cescutti, P.; Tossi, A.; Rizzo, R. Inhibition of cathelicidin activity by bacterial exopolysaccharides. *Mol. Microbiol.* **2009**, *72*, 1137–1146. [[CrossRef](#)]
61. Zhu, C.; Mu, X.; Van Aken, P.A.; Maier, J.; Yu, Y. Fast Li storage in MoS₂-graphene-carbon nanotube nanocomposites: Advantageous functional integration of 0D, 1D, and 2D nanostructures. *Adv. Energy Mater.* **2015**, *5*, 1–8. [[CrossRef](#)]
62. Radisavljevic, B.; Radenovic, A.; Brivio, J.; Giacometti, V.; Kis, A. Single-layer MoS₂ transistors. *Nat. Nanotechnol.* **2011**, *6*, 147–150. [[CrossRef](#)] [[PubMed](#)]
63. Adamczyk, Z.; Weroński, P. Application of the DLVO theory for particle deposition problems. *Adv. Colloid Interface Sci.* **1999**, *83*, 137–226. [[CrossRef](#)]
64. Perni, S.; Preedy, E.C.; Prokopovich, P. Success and failure of colloidal approaches in adhesion of microorganisms to surfaces. *Adv. Colloid Interface Sci.* **2014**, *206*, 265–274. [[CrossRef](#)] [[PubMed](#)]
65. Putz, K.W.; Compton, O.C.; Segar, C.; An, Z.; Nguyen, S.T.; Brinson, L.C. Evolution of order during vacuum-assisted self-assembly of graphene oxide paper and associated polymer nanocomposites. *ACS Nano* **2011**, *5*, 6601–6609. [[CrossRef](#)] [[PubMed](#)]
66. Xu, K.; Chen, W.; Fu, G.; Mou, X.; Hou, R.; Zhu, Y.; Cai, K. In situ self-assembly of graphene oxide/polydopamine/Sr²⁺ nanosheets on titanium surfaces for enhanced osteogenic differentiation of mesenchymal stem cells. *Carbon N. Y.* **2019**, *142*, 567–579. [[CrossRef](#)]
67. Gigantelli, J.W.; Torres Gomez, J.; Osato, M.S. In vitro susceptibilities of ocular *Bacillus cereus* isolates to clindamycin, gentamicin, and vancomycin alone or in combination. *Antimicrob. Agents Chemother.* **1991**, *35*, 201–202. [[CrossRef](#)]
68. Field, T.R.; White, A.; Elborn, J.S.; Tunney, M.M. Effect of oxygen limitation on the in vitro antimicrobial susceptibility of clinical isolates of *Pseudomonas aeruginosa* grown planktonically and as biofilms. *Eur. J. Clin. Microbiol. Infect. Dis.* **2005**, *24*, 677–687. [[CrossRef](#)] [[PubMed](#)]
69. Zhang, X.; Jia, F.; Yang, B.; Song, S. Oxidation of Molybdenum Disulfide Sheet in Water under in Situ Atomic Force Microscopy Observation. *J. Phys. Chem. C* **2017**, *121*, 9938–9943. [[CrossRef](#)]
70. Hakobyan, K.Y.; Sohn, H.Y.; Hakobyan, A.K.; Bryukvin, V.A.; Leontiev, V.G.; Tsibin, O.I. The oxidation of molybdenum sulphide concentrate with water vapour Part 1—Thermodynamic aspects. *Trans. Inst. Min. Metall. Sect. C Miner. Process. Extr. Metall.* **2013**, *116*, 152–154. [[CrossRef](#)]
71. Pandit, S.; Karunakaran, S.; Boda, S.K.; Basu, B.; De, M. High antibacterial activity of functionalized chemically exfoliated MoS₂. *ACS Appl. Mater. Interfaces* **2016**, *8*, 31567–31573. [[CrossRef](#)]
72. Lushchak, V.I. Adaptive response to oxidative stress: Bacteria, fungi, plants and animals. *Comp. Biochem. Physiol. C Toxicol. Pharmacol.* **2011**, *153*, 175–190. [[CrossRef](#)]

73. Desriac, N.; Broussolle, V.; Postollec, F.; Mathot, A.G.; Sohier, D.; Coroller, L.; Leguerinel, I. Bacillus cereus cell response upon exposure to acid environment: Toward the identification of potential biomarkers. *Front. Microbiol.* **2013**, *4*, 1–13. [[CrossRef](#)]
74. Duport, C.; Jobin, M.; Schmitt, P. Adaptation in *Bacillus cereus*: From stress to disease. *Front. Microbiol.* **2016**, *7*, 1–18. [[CrossRef](#)] [[PubMed](#)]
75. Mols, M.; Abee, T. *Bacillus cereus* responses to acid stress. *Environ. Microbiol.* **2011**, *13*, 2835–2843. [[CrossRef](#)]
76. Goepfert, J.M.; Spira, W.M.; Kim, H.U. Bacillus cereus: Food poisoning organism. A review. *J. Milk Food Technol.* **1972**, *35*, 213–227. [[CrossRef](#)]
77. Bushell, F.M.L.; Tonner, P.D.; Jabbari, S.; Schmid, A.K.; Lund, P.A. Synergistic impacts of organic acids and pH on growth of *Pseudomonas aeruginosa*: A comparison of parametric and Bayesian non-parametric methods to model growth. *Front. Microbiol.* **2019**, *10*, 1–15. [[CrossRef](#)] [[PubMed](#)]
78. Titley, S.R. Some behavioral aspects of molybdenum in the supergene environment. *Trans. AIME* **1963**, *226*, 199–204.
79. Wagman, D.D. *Selected Values of Chemical Thermodynamic Properties*; Institute for Materials Research, National Bureau of Standards: Gaithersburg, MA, USA, 1965; Volume 270.
80. Liu, X.; Cheng, J.; Sprik, M.; Lu, X. Solution structures and acidity constants of molybdic acid. *J. Phys. Chem. Lett.* **2013**, *4*, 2926–2930. [[CrossRef](#)]
81. Bae, M. Molybdenum Disulfide 2-D Nanosheets Toxicology to the Environmental Surfaces: Soil Bacteria Survivability Analysis. Master's Thesis, Texas A&M University, College Station, TX, USA, 2017.